Energy-Aware 3D UAV Path Planning in Mountainous Terrain via TDAMSO

Li Tan[1]*, Jiaqin Chai[1], Dongjiao Ge[2], Ruimeng Tian[1], Xinshi Zhang[1]
[1] School of Computer and Artificial Intelligence, Beijing Technology and Business University, Beijing, China
[2] Faculty of Data Science, City University of Macau, Macau (SAR), China
Email: *tanli@th.btbu.edu.cn, {2431062117, zhangxinshi}@st.btbu.edu.cn, djge@cityu.edu.mo, 3275957378@qq.com

***Abstract*—Unmanned Aerial Vehicles (UAVs) are increasingly deployed in energy-intensive transportation tasks. While UAVs enable rapid access in mountainous regions, rugged topography and dense obstacles make 3D path planning a high-dimensional, heavily constrained problem. Under strict safety and feasibility requirements, many existing methods converge slowly and yield high-cost trajectories, increasing energy consumption under battery-limited operations. To address these challenges, this paper proposes Thermal-conduction Dynamic Adaptive Mirage Search Optimization (TDAMSO) for energy-aware planning in complex mountainous environments. TDAMSO integrates Sobol low-discrepancy sequence initialization, a differential thermal-conduction search strategy, nonlinear dynamic step-size adjustment, and an adaptive Cauchy-Gaussian dual-layer local search to accelerate convergence and reduce the overall path cost. Moreover, an energy-oriented 3D path cost model is constructed to unify flight distance, climbing, turning, and smoothness costs, along with terrain and obstacle-related safety constraints. The planned trajectories provide a reusable primitive for mission energy budgeting and green aerial logistics under safety constraints. Multi-scenario simulations show that TDAMSO outperforms other representative metaheuristics and advanced optimization algorithms in terms of total energy-related cost, obstacle-avoidance feasibility, and convergence speed. Overall, TDAMSO provides an effective and reliable approach for energy-efficient UAV transportation in complex terrain.**

***Index Terms*—UAV path planning, mirage search optimization, energy-aware navigation, mountainous terrain.**

I. Introduction

Mountainous regions are characterized by complex terrain and limited accessibility, where disasters such as landslides and collapses often hinder timely response [1]. UAVs have been widely adopted for emergency reconnaissance, delivery, and communication relay due to their rapid deployment and terrain adaptability. However, frequent climbs and detours in rugged environments significantly increase energy consumption and reduce endurance. Therefore, energy-aware path planning is essential to ensure safe and efficient UAV operations [2].

Existing UAV path planning methods mainly include traditional and metaheuristic approaches [3]. Traditional methods rely on accurate environmental modeling, but often struggle with efficiency and global optimality in complex terrains. Metaheuristic algorithms provide flexible continuous-space search, yet may suffer from local optima entrapment and unstable convergence in high-dimensional, constrained environments. Consequently, generating feasible, energy-efficient, and smooth trajectories with stable convergence remains a critical challenge in 3D mountainous path planning.

To address this challenge, this paper proposes TDAMSO, an enhanced Mirage Search Optimization (MSO) [4] framework. By integrating multiple cooperative strategies, TDAMSO improves population diversity, global exploration, adaptive convergence control, and local refinement. As a result, it achieves faster and more stable convergence within a fixed iteration budget, leading to lower path cost and reduced variability, thereby supporting energy-aware UAV path planning. The main contributions are summarized as follows.

- We propose TDAMSO, an enhanced MSO framework integrating Sobol initialization, differential thermal-conduction search, nonlinear dynamic step-size control, and adaptive Cauchy-Gaussian dual-layer local search to improve convergence efficiency and robustness under strong constraints, thereby reducing the overall energy-proxy path cost.
- We construct an energy-oriented three-dimensional path planning cost model that couples energy proxy terms (flight distance, climbing, and turning) with terrain and obstacle-related safety constraints, altitude limits, and trajectory executability constraints.
- We conduct extensive simulations in multiple complex mountainous environments to validate the proposed method in terms of total energy-related cost, convergence stability, and collision-free feasibility.

II. Related Work

Over the past few decades, extensive research has explored various methodologies for optimal path planning. Traditional approaches are often categorized into global planning and online replanning methods according to their reliance on environmental information and operational scope. Global planners, represented by A* [5], Dijkstra [6], and Rapidly-exploring Random Trees (RRT) [7], construct feasible paths using a priori maps, whereas online replanning methods such as the Artificial Potential Field (APF) [8] and D* Lite [9] emphasize real-time adjustments in dynamic environments. However, in complex 3D mountainous environments and energy-sensitive transportation tasks, stringent safety and feasibility constraints

* Corresponding author.

substantially increase planning difficulty and search overhead, causing traditional planning methods to struggle to meet both feasibility and solution quality under limited optimization budgets, which frequently leads to suboptimal path generation in real-world mission scenarios.

In contrast, metaheuristic approaches perform continuous-space search by simulating collective behaviors and have been widely applied to complex path planning due to their robustness and simple implementation [10]. Representative examples include Particle Swarm Optimization (PSO) [11], Crested Porcupine Optimizer (CPO) [12], and the Whale Optimization Algorithm (WOA) [13]. To mitigate slow convergence and stagnation in local optima, various hybridization and multi-strategy enhancements have been proposed. Fan *et al.* [14] developed a nature-inspired adaptive Differential Evolution (DE) framework with a golden-section strategy for high-dimensional planning. Chen *et al.* [15] incorporated Artificial Potential Field (APF) guidance as a hybrid strategy. For obstacle avoidance in complex environments, Yang *et al.* [16] introduced a Cauchy mutation operator into the Marine Predator Algorithm (MPA) to improve optimization accuracy in 3D spaces. Regarding terrain adaptability, Zhou *et al.* [17] incorporated Levy flight into the Pelican Optimization Algorithm (POA) to better balance path distance, energy consumption, and threat costs in rugged terrain; Wang *et al.* [18] proposed an Arithmetic Optimization Algorithm (AOA) under a global-dynamic programming model to maintain the exploration–exploitation balance. Despite progress in specific scenarios, performance often remains sensitive to initialization quality, and multimodal, high-dimensional constrained spaces can still induce unstable convergence and inefficient search behavior, limiting reliable decision-making for energy-intensive transportation tasks [19]. Consequently, there is a pressing need for advanced mechanisms that can effectively balance the exploration of the global search space with the exploitation of promising local regions to ensure consistent trajectory quality.

Overall, in obstacle-dense mountainous environments, planners often fail to deliver energy-economical, executable trajectories with fast, stable convergence under limited budgets, undermining mission energy budgeting. Motivated by this gap, we target robust convergence toward low-energy, smooth, and feasible trajectories to support energy-aware transportation.

III. MATHEMATICAL MODEL

A. Mountain Terrain Modeling

The mountainous environment is modeled as a continuous height field with a four-layer structure(see Fig. 1):

$$h(x, y) = h_{\text{base}}(x, y)+h_{\text{peaks}}(x, y)+h_{\text{ridges}}(x, y)+h_{\text{noise}}(x, y) \tag{1}$$

where h_{base} captures large-scale elevation trends, h_{peaks} and h_{ridges} simulate local mountainous summits and elongated ridge structures, respectively, and h_{noise} introduces fine-scale terrain irregularities.

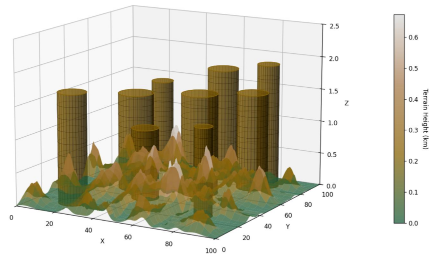

Fig. 1. 3D mountainous planning environment consisting of a $100 \times 100 \times 2.5$ km terrain surface with color-coded elevation (dark green: low, brown: high) and cylindrical no-fly obstacles.

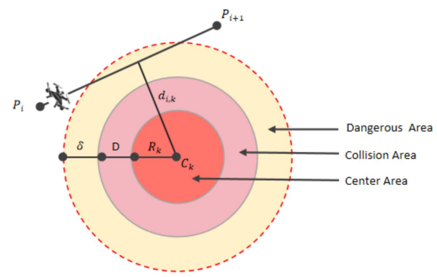

Fig. 2. Top view of the obstacle threat area

B. Path Cost Model

A composite cost function is defined to balance energy efficiency, flight safety, and trajectory feasibility, consisting of five terms: distance, maneuver, smoothness, threat, and height.

1) Flight Path Length Cost: For a path with n nodes $\mathbf{p}_i = (x_i, y_i, z_i)$, the distance cost is:

$$J_{\text{dist}} = \sum_{i=1}^{n-1} \|\mathbf{p}_{i+1} - \mathbf{p}_i\|_2 \tag{2}$$

2) Climb and Turn Maneuver Cost: Frequent climbing and sharp turning consume additional energy. A lightweight proxy is adopted:

$$J_{\text{maneuver}} = \sum_{i=1}^{n-1} \lambda_h \max(0, \Delta h_i) + \sum_{i=2}^{n-1} \lambda_\theta \theta_i^2 \tag{3}$$

where $\Delta h_i = z_{i+1} - z_i$ (climbing penalty only when $\Delta h_i > 0$), θ_i is the turning angle. λ_h and λ_θ weight the climbing and turning contributions, respectively.

3) Flight Path Smoothing Cost: To improve motion continuity and suppress zig-zag artifacts that cause control oscillations, a geometric smoothness regularizer is introduced.

$$J_{\text{smooth}} = \sum_{i=2}^{n-1} \|\mathbf{p}_{i+1} - 2\mathbf{p}_i + \mathbf{p}_{i-1}\|_2 \tag{4}$$

4) Threat Minimization Cost: To account for collision risks from obstacles, the threat cost is defined as the sum of a node-based term and a segment-based intersection term (see Fig. 2):

$$J_{\text{threat}} = J_{\text{point}} + J_{\text{seg}} \tag{5}$$

Obstacle Proximity and Collision Cost: For each node, a collision penalty C_1 is applied if the node lies inside the collision area, and a buffer penalty C_2 if it lies within the dangerous area.

$$J_{\text{point}} = \sum_{i=1}^{n} \sum_{k=1}^{N_o} \begin{cases} C_1, & d_{i,k} \leq R_k + D, \\ C_2, & R_k + D < d_{i,k} \leq R_k + D + \delta, \\ 0, & \text{otherwise.} \end{cases} \tag{6}$$

where N_o is the number of obstacles, $d_{i,k}$ is the horizontal distance to obstacle k (radius R_k), D is the UAV diameter, and δ is the safety buffer.

Segment-obstacle Intersection Cost: For a segment L_i with horizontal projection $\Pi(L_i)$ and obstacle k with footprint Ω_k and height range $[z_k^{\min}, z_k^{\max}]$, define $A_{i,k} = \mathbb{I}(\Pi(L_i) \cap \Omega_k \neq \emptyset)$ and $B_{i,k} = \mathbb{I}([\min(z_i, z_{i+1}), \max(z_i, z_{i+1})] \cap [z_k^{\min}, z_k^{\max}] \neq \emptyset)$. If $A_{i,k}B_{i,k} = 1$, the segment intersects the obstacle in 3D. Then:

$$J_{\text{seg}} = \sum_{i=1}^{n-1} \sum_{k=1}^{N_o} C_3 \, A_{i,k} B_{i,k}, \tag{7}$$

where C_3 is the penalty coefficient.

5) Flight Height Feasibility Cost: The UAV must stay above terrain and below a maximum altitude:

$$J_{\text{height}} = \sum_{i=1}^{n} \begin{cases} \infty, & z_i \leq h(x_i, y_i) + \delta_{\text{safe}}, \\ 10 \cdot (z_i - h_{\max}), & z_i > h_{\max}, \\ 0, & \text{otherwise.} \end{cases} \tag{8}$$

where $h(x_i, y_i)$ is the terrain elevation, z_i is the UAV altitude, $\delta_{\text{safe}} = 0.02$ km and $h_{\max}$ is the maximum allowed altitude.

6) Total Cost Function: The overall objective is formulated as a weighted sum:

$$J_{\text{Cost}} = w_D J_{\text{dist}} + w_M J_{\text{maneuver}} + w_S J_{\text{smooth}} + w_T J_{\text{threat}} + w_O J_{\text{height}} \tag{9}$$

J_{dist} serves as the primary proxy for energy consumption; the maneuver and smoothness terms suppress high-energy and unstable motions; the threat and height terms enforce safety. All components are normalized, and fixed weights are used across all scenarios.

IV. MAIN ALGORITHM

This section introduces TDAMSO, an improved Mirage Search Optimization algorithm for energy-aware 3D UAV path planning that integrates four key enhancement modules. These modules accelerate and stabilize convergence in constrained spaces, reducing the energy-proxy cost and supporting reliable mission energy budgeting. The overall framework of TDAMSO is shown in Fig. 3.

A. Sobol Low-discrepancy Sequence Initialization

The original MSO adopts random initialization, which may lead to uneven population distribution and limited diversity, increasing the risk of premature convergence. To address this issue, an initialization scheme based on Sobol low-discrepancy sequences [20] is employed to improve population uniformity and early-stage exploration. The initialization is defined as:

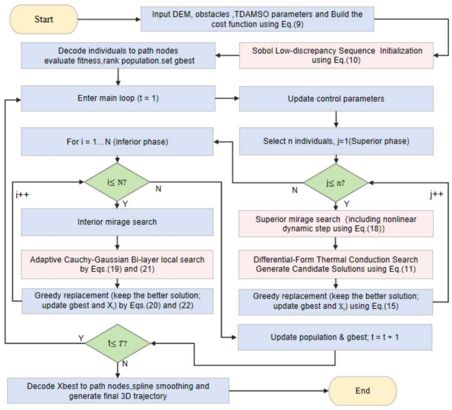

Fig. 3. Framework of TDAMSO for energy-aware 3D UAV path planning in mountainous environments

$$\mathbf{X}_i = \mathbf{lb} + \mathbf{S}_i \odot (\mathbf{ub} - \mathbf{lb}), \quad i = 1, 2, \ldots, N \tag{10}$$

where $\mathbf{S}_i \in [0,1]^{\text{Dim}}$ is the Sobol sample, $\mathbf{ub}$ and $\mathbf{lb}$ are the upper and lower bounds, N indicates the population size, and Dim refers to the dimensionality of the search space.

B. Differential Thermal-conduction Search

To enhance exploration, a differential thermal-conduction search (Diff-Tcs) strategy is introduced based on the thermal-conduction search mechanism in [18]. By incorporating differential interaction, Diff-Tcs combines elite guidance and population-level diffusion to improve global search capability.

In the t-th iteration, the candidate solution of the i-th individual is updated as:

$$\mathbf{x}_i^{\text{Tcs},t+1} = \mathbf{x}_i^t + \kappa_t \left(\mathbf{x}_{\text{best}}^t - \mathbf{x}_i^t\right) + \mu_t \left(\mathbf{x}_{\text{mean}}^t - \mathbf{x}_i^t\right) + \mathbf{tr}_i' \tag{11}$$

$$\kappa_t = \kappa_{\text{final}} + \frac{\kappa_{\text{init}} - \kappa_{\text{final}}}{1 + \exp\big(0.02\,(t - T/2)\big)} \tag{12}$$

$$\mu_t = \mu_{\text{final}} + (\mu_{\text{init}} - \mu_{\text{final}}) \left(1 - \frac{t}{T}\right) \tag{13}$$

$$\mathbf{tr}_i' = \delta \cdot \left(\text{tr}_{\text{scale}} \left(\mathbf{ub} - \mathbf{lb}\right)\right) \odot \mathbf{t}_i', \qquad \mathbf{t}_i' \sim t_{df}(\mathbf{0}, \mathbf{I}) \tag{14}$$

where $\mathbf{x}_i^t$ is the current position, $\mathbf{x}_{\text{best}}^t$ and $\mathbf{x}_{\text{mean}}^t$ denote the global best and population mean, respectively. The coefficients κ_t and μ_t control the contributions of elite guidance and diffusion, and gradually decrease over iterations to balance exploration and convergence. $\kappa_{\text{init}} = 0.9$, $\kappa_{\text{final}} = 0.1$, $\mu_{\text{init}} = 0.16$, $\mu_{\text{final}} = 0.12$, and T is the maximum number of iterations. The perturbation term $\mathbf{tr}_i'$ follows a heavy-tailed t-distribution, enabling occasional long jumps to escape local optima.

Each individual generates two candidates, $\mathbf{x}_i^{\text{up},t+1}$ and $\mathbf{x}_i^{\text{Tcs},t+1}$, and the better one is selected by:

$$\mathbf{x}_i^{t+1} = \begin{cases} \mathbf{x}_i^{\text{up},t+1}, & \text{if } f\left(\mathbf{x}_i^{\text{up},t+1}\right) \leq f\left(\mathbf{x}_i^{\text{Tcs},t+1}\right), \\ \mathbf{x}_i^{\text{Tcs},t+1}, & \text{otherwise.} \end{cases} \tag{15}$$

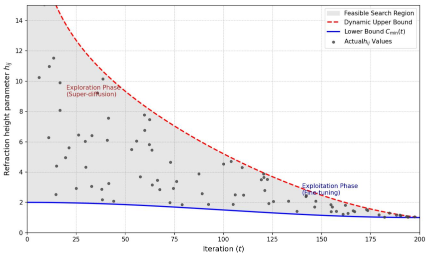

Fig. 4. The range of values for the refraction height (h_{ij}) parameter.

C. Nonlinear Dynamic Step-size Adjustment

To adapt the search scale across different iteration stages, a nonlinear dynamic step-size mechanism is introduced in the superior mirage phase. The lower-bound term is modeled by a cosine-based schedule $C_{\min}(t)$, while the step size is controlled by a quadratically decaying factor $\lambda(t)$, enabling a smooth transition from exploration to refinement.

$$C_{\min}(t) = 1 + \frac{1 + \cos(\pi \cdot \frac{t}{T})}{2} \tag{16}$$

$$\lambda(t) = \lambda_{\min} + (\lambda_{\max} - \lambda_{\min}) \left(1 - \left(\frac{t}{T}\right)^2\right) \tag{17}$$

where $\lambda_{\max} = 8$ and $\lambda_{\min} = 3$. The refraction height h_{ij} is adaptively bounded as:

$$C_{\min}(t) \leq h_{ij} \leq \lambda(t) \cdot \operatorname{arctanh}\left(1 - \frac{t}{T}\right) + C_{\min}(t) \tag{18}$$

As shown in Fig. 4, the feasible range of h_{ij} shrinks over iterations, facilitating a smooth transition from global exploration to local refinement.

D. Adaptive Cauchy–Gaussian Dual-layer Local Search Mechanism

An adaptive dual-layer local search is introduced in the inferior mirage phase to enhance solution refinement. The mechanism integrates Cauchy mutation for global perturbation and Gaussian perturbation for elite exploitation, forming a coarse-to-fine search process.

In the first layer, a Cauchy mutation is applied:

$$\mathbf{x}_i^{\mathrm{C},t+1} = \mathbf{x}_i^{\mathrm{low},t+1} + \alpha_c\, e^{\left(1-\frac{t}{T}\right)} \left(\mathbf{x}_i^{\mathrm{low},t+1} \odot \mathrm{C}(0,1)\right) \tag{19}$$

$$\mathbf{x}_i^{t+1} = \begin{cases} \mathbf{x}_i^{\mathrm{low},t+1}, & \text{if } f\left(\mathbf{x}_i^{\mathrm{low},t+1}\right) \leq f\left(\mathbf{x}_i^{\mathrm{C},t+1}\right), \\ \mathbf{x}_i^{\mathrm{C},t+1}, & \text{otherwise.} \end{cases} \tag{20}$$

where $\mathbf{x}_i^{\mathrm{low},t+1}$ is the base solution after the inferior mirage update, $\mathrm{C}(0,1)$ denotes the standard Cauchy distribution. α_c indicates the Cauchy mutation intensity, which is set to 0.15. Subsequently, the candidate solution generated via Cauchy mutation $x_i^{\mathrm{C},t+1}$ is compared with the base solution.

In the second layer, the top 10% individuals form the elite set E_t, and a Gaussian refinement is applied:

$$\mathbf{x}_i^{G,t+1} = \mathbf{x}_i^{t+1} + \boldsymbol{\varepsilon}_i, \boldsymbol{\varepsilon}_i \sim \mathcal{N}(\mathbf{0}, \sigma^2\mathbf{I}), \quad \sigma = 0.1. \tag{21}$$

$$\mathbf{x}_i^{t+1} = \begin{cases} \mathbf{x}_i^{G,t+1}, & \text{if } f(\mathbf{x}_i^{G,t+1}) \leq f(\mathbf{x}_i^{t+1}), \\ \mathbf{x}_i^{t+1}, & \text{otherwise.} \end{cases} \tag{22}$$

where $i \in E_t$. This mechanism improves solution quality by combining large-step exploration with fine-grained local refinement. $\mathbf{I}$ is the identity matrix, and $\boldsymbol{\varepsilon}_i$ is a zero-mean Gaussian perturbation vector.

V. EXPERIMENTS AND RESULTS

A. Experimental Setup

Five 3D path-planning scenarios of increasing difficulty are designed over a fixed mountainous terrain by varying the number and layout of cylindrical obstacles. All algorithms minimize Eq. (9), which serves as an energy-proxy objective under safety constraints. Mean path length is also reported, as flight distance is a primary contributor to UAV energy consumption. Convergence curves reflect convergence speed and solution quality, where faster and stabler convergence reduces optimization overhead. The population size is 30, the maximum iterations is 200, and each algorithm is independently run 20 times per scenario. The start point $(0, 0, 0)$ and goal point $(100, 90, 0)$ are marked by a triangle and a circle, with different colors representing different algorithms. All simulations are implemented in Python on a PC with an AMD Ryzen 5 4500U CPU and 16 GB RAM.

B. Comparative Experiment

To assess the effectiveness and feasibility of the proposed TDAMSO, we compare it with several representative meta-heuristics, including the original MSO, CPO, WOA, DE, GA, and PSO. The parameter settings are summarized in Table I. Figs. 5–8 illustrate representative planned paths for Scenarios 1–4. Table II reports the mean cost, the best cost, the standard deviation, and the mean path length over 20 independent runs, where the mean total cost determines the rank.

As shown in Fig. 5, all methods can generate feasible collision-free paths from start to goal. However, PSO and GA produce noticeable detours and large altitude oscillations, leading to a higher total cost. By contrast, TDAMSO yields a more compact trajectory with reasonable clearance margins and smoother altitude variations, achieving both safety and lower energy-related cost.

The convergence curves and statistics in Figs. 6 and 7 further indicate that TDAMSO descends faster in the early iterations and reaches a stable plateau with fewer iterations, suggesting that high-quality solutions can be obtained with reduced search overhead. The box plots show a more concentrated cost distribution for TDAMSO, with a lower median, smaller dispersion, and fewer outliers, demonstrating improved robustness across runs.

Under stronger constraints and narrower passages (Fig. 8), the baseline methods generally converge more slowly and exhibit larger cost fluctuations. Some of them avoid obstacles by excessive climbs or redundant detours, which increases the energy-related cost. In contrast, TDAMSO maintains rapid

TABLE I

PARAMETER SETTINGS OF THE COMPARED ALGORITHMS.

Algorithm	Parameter	Value
TDAMSO	$C_{\min}$	Nonlinear reduction 2 to 1
MSO	$C_{\min}$	1
DE	Scaling factor (F) Crossover probability (P_c)	0.5 0.9
GA	Crossover probability (P_c) Mutation probability (P_m)	0.7 0.1
PSO	Inertia weight (ω) Cognitive coefficient (C_1) Social coefficient (C_2)	0.5 1.0 1.0
CPO	T_f α	0.8 0.2
WOA	b	1

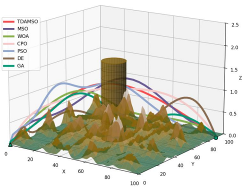

(a) 3D track

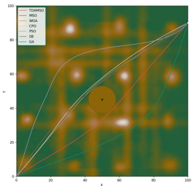

(b) Top view

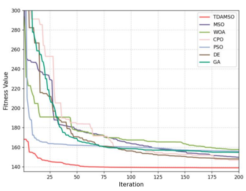

(c) Convergence curve

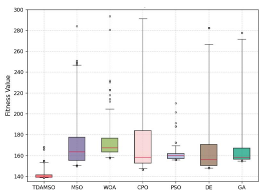

(d) Box plot

Fig. 5. The results generated by the seven algorithms in Scenario 1.

convergence and achieves lower and more stable fitness values, demonstrating its advantage in producing low-energy paths with efficient decision-making in complex mountainous terrain.

C. Ablation Experiment

To assess the contributions of individual TDAMSO modules to energy-efficient path planning, we conduct an ablation study in Scenario 5 by comparing TDAMSO with the original MSO and four single-strategy variants: (i) SMSO (Sobol low-discrepancy sequence initialization), (ii) TMSO (differential thermal-conduction search), (iii) DMSO (nonlinear dynamic step-size adjustment), and (iv) AMSO (adaptive Cauchy-Gaussian dual-layer local search). As shown in Fig. 9 and Table III, SMSO increases early-stage feasibility and reduces invalid evaluations; TMSO strengthens global exploration to mitigate local-optimum-induced detours; DMSO improves mid-to-late step-size allocation to enhance convergence stability; and AMSO refines final-stage candidates to suppress oscillations and further shorten the path. Overall, TDAMSO achieves the best convergence speed and final cost with the

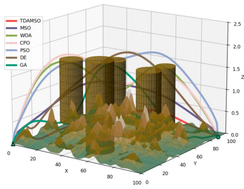

(a) 3D track

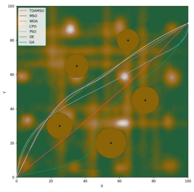

(b) Top view

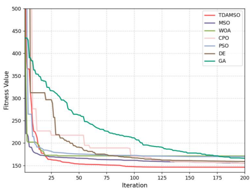

(c) Convergence curve

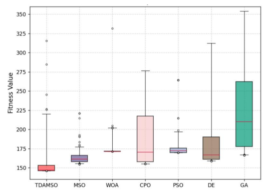

(d) Box plot

Fig. 6. The results generated by the seven algorithms in Scenario 2.

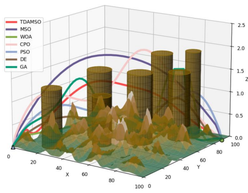

(a) 3D track

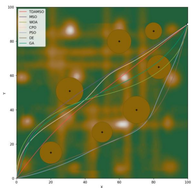

(b) Top view

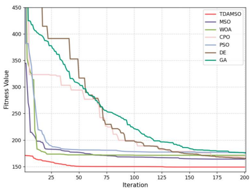

(c) Convergence curve

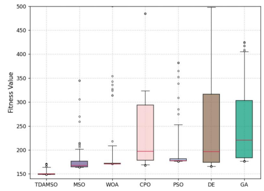

(d) Box plot

Fig. 7. The results generated by the seven algorithms in Scenario 3.

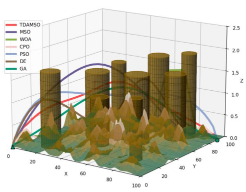

(a) 3D track

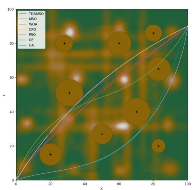

(b) Top view

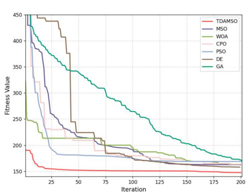

(c) Convergence curve

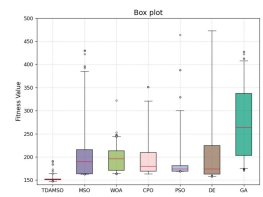

(d) Box plot

Fig. 8. The results generated by the seven algorithms in Scenario 4.

TABLE II

COMPARISON OF COST AND PATH LENGTH METRICS.

Scenario	Metric	TDAMSO	MSO	WOA	CPO	PSO	DE	GA
1	**Cost.mean**	**139.9076**	145.9723	157.4847	146.9412	154.0737	146.5919	153.0380
	Cost.std	**0.4442**	8.3226	11.2741	4.3313	7.0473	6.1501	9.0121
	Cost.best	139.1768	**138.3458**	139.3976	142.0292	145.6004	139.7227	140.3339
	Len.mean	**135.7500**	135.9290	136.8144	137.0856	137.1896	136.0845	139.0585
2	**Cost.mean**	**143.1336**	154.6372	171.1847	153.9893	173.5762	157.6783	169.6127
	Cost.std	**7.5801**	12.0193	22.4664	8.5958	17.6476	12.2598	28.3845
	Cost.best	**136.4327**	136.4470	138.1040	140.1669	153.6183	139.9161	141.6503
	Len.mean	135.9275	142.1938	**135.2130**	138.6343	149.3657	144.9392	147.4459
3	**Cost.mean**	**145.2866**	159.6070	171.0838	168.0752	181.6790	166.3520	174.4203
	Cost.std	**2.1901**	14.7768	25.6338	10.4204	19.8149	19.1644	19.8625
	Cost.best	141.0875	**139.4548**	140.4885	153.6397	145.2435	149.5640	145.6835
	Len.mean	**135.2632**	146.8301	142.4926	142.4157	156.3924	147.1223	147.2089
4	**Cost.mean**	**144.7216**	162.7187	164.5025	163.9168	177.5135	160.2606	170.7486
	Cost.std	**5.9893**	13.4855	18.6904	12.3717	20.4402	17.1209	18.6857
	Cost.best	**137.9078**	138.8477	140.0754	143.6574	146.9515	139.3138	143.7669
	Len.mean	**135.3585**	146.8439	140.4156	143.0229	158.0831	146.2500	149.6331
	Rank	**1**	2	6	4	7	3	5

TABLE III

COMPARISON OF COST AND PATH LENGTH METRICS IN SCENARIO 5.

Scenario	Metric	TDAMSO	MSO	SMSO	TMSO	DMSO	AMSO
5	**Cost.mean**	**141.9971**	162.1130	152.8853	152.2650	160.9000	157.1292
	Cost.std	**8.0620**	24.2061	20.6788	18.9361	14.9500	15.2648
	Cost.best	**135.8982**	138.7513	135.9720	136.4053	137.7607	136.1720
	Len.mean	**135.6475**	146.1130	141.2116	143.1476	140.4490	143.0068

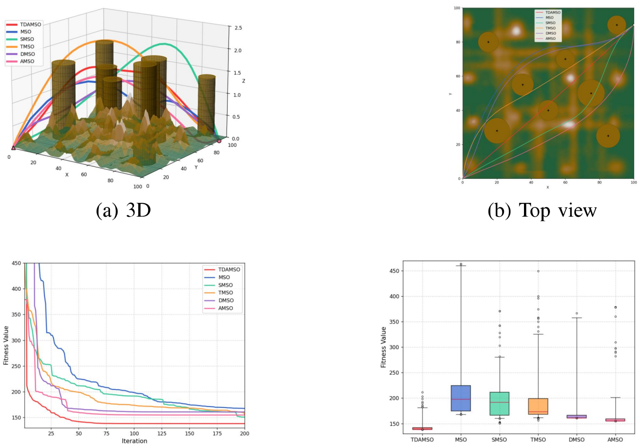

(a) 3D

(b) Top view

(c) Convergence curve

(d) Box plot

Fig. 9. The results generated by the six algorithms in Scenario 5.

smallest dispersion, indicating that these modules act synergistically along a pipeline of "feasibility enhancement-global exploration-stage-wise convergence-local refinement" to yield shorter and more energy-efficient paths.

VI. CONCLUSIONS

This paper proposes TDAMSO, an enhanced Mirage Search Optimization algorithm for energy-aware 3D UAV path planning in complex mountainous environments. By integrating Sobol initialization, differential thermal-conduction search, nonlinear step-size control, and adaptive Cauchy-Gaussian local search, it improves convergence efficiency and reduces path cost, thereby lowering energy consumption. Results show that TDAMSO generates feasible and smooth trajectories in obstacle-dense scenarios with superior performance over baseline algorithms. Future work will address dynamic environments and refined energy modeling.

VII. ACKNOWLEDGMENT

This work was supported by the National Natural Science Foundation of China under Grant 62472010.

REFERENCES

[1] H. Zhou, A. Che, and G. Li, "Characteristics and failure mechanism of landslides along highways triggered by 2021 ms6.4 yangbi earthquake," *Landslides*, vol. 19, no. 1, pp. 165–176, 2022.

[2] S. Aggarwal and N. Kumar, "Path planning techniques for unmanned aerial vehicles: A review, solutions, and challenges," *Computer Communications*, vol. 149, pp. 270–299, 2020.

[3] P. Kumar, K. Pal, and M. C. Govil, "Comprehensive review of path planning techniques for unmanned aerial vehicles (uavs)," *ACM Computing Surveys*, vol. 58, no. 3, pp. 1–44, 2025.

[4] J. He, S. Zhao, J. Ding, and Y. Wang, "Mirage search optimization: Application to path planning and engineering design problems," *Advances in Engineering Software*, vol. 203, p. 103883, 2025.

[5] Z. Li, Z. Chen, W. Wu, B. Chen, Y. Zhan, and J. Dong, "An emergency path planning method for UAV based on A* algorithm," in *2024 5th International Conference on Information Science, Parallel and Distributed Systems (ISPDS)*. IEEE, 2024, pp. 540–544.

[6] C. Wang, C. Cheng, D. Yang, G. Pan, and F. Zhang, "Path planning in localization uncertaining environment based on Dijkstra method," *Frontiers in Neurorobotics*, vol. 16, p. 821991, 2022.

[7] B. Li and B. Chen, "An adaptive rapidly-exploring random tree," *IEEE/CAA Journal of Automatica Sinica*, vol. 9, no. 2, pp. 283–294, 2021.

[8] Y. Sun, W. Chen, and J. Lv, "UAV path planning based on improved artificial potential field method," in *2022 International Conference on Computer Network, Electronic and Automation (ICCNEA)*. IEEE, 2022, pp. 95–100.

[9] J. Yu, M. Yang, Z. Zhao, X. Wang, Y. Bai, J. Wu, and J. Xu, "Path planning of unmanned surface vessel in an unknown environment based on improved D* Lite algorithm," *Ocean Engineering*, vol. 266, p. 112873, 2022.

[10] A. Alorf, "A survey of recently developed metaheuristics and their comparative analysis," *Engineering Applications of Artificial Intelligence*, vol. 117, p. 105622, 2023.

[11] Z. Yu, Z. Si, X. Li, D. Wang, and H. Song, "A novel hybrid particle swarm optimization algorithm for path planning of UAVs," *IEEE Internet of Things Journal*, vol. 9, no. 22, pp. 22 547–22 558, 2022.

[12] M. Abdel-Basset, R. Mohamed, and M. Abouhawwash, "Crested porcupine optimizer: A new nature-inspired metaheuristic," *Knowledge-Based Systems*, vol. 284, p. 111257, 2024.

[13] L. Deng and S. Liu, "Deficiencies of the whale optimization algorithm and its validation method," *Expert Systems with Applications*, vol. 237, p. 121544, 2024.

[14] S. Fan, R. Wang, Y. Song, D. Crosbee, and K. Su, "Nature-inspired adaptive differential evolution: A unified meta-heuristic framework for complex engineering optimisation and uav path planning," *Results in Engineering*, p. 106530, 2025.

[15] Y. Chen, Q. Yu, D. Han, and H. Jiang, "UAV path planning: Integration of grey wolf algorithm and artificial potential field," *Concurrency and Computation: Practice and Experience*, vol. 36, no. 15, p. e8120, 2024.

[16] L. Lyu and F. Yang, "MMPA: A modified marine predator algorithm for 3D UAV path planning in complex environments with multiple threats," *Expert Systems with Applications*, vol. 257, p. 124955, 2024.

[17] G. Zhou, S. Lü, L. Mao, K. Xu, T. Bao, and X. Bao, "Path planning of UAV using levy pelican optimization algorithm in mountain environment," *Applied Artificial Intelligence*, vol. 38, no. 1, p. 2368343, 2024.

[18] W. Wang and J. Tian, "Dynamic UAV path planning in mountainous terrain utilizing an arithmetic optimization algorithm incorporating adaptive thermal conduction search and elite population genetic strategies," *Aerospace Science and Technology*, p. 110950, 2025.

[19] B. Li, Q. Li, Y. Zeng, Y. Rong, and R. Zhang, "3D trajectory optimization for energy-efficient UAV communication: A control design perspective," *IEEE Transactions on Wireless Communications*, vol. 21, no. 6, pp. 4579–4593, 2021.

[20] X. Sun, B. Croke, S. Roberts, and A. Jakeman, "Comparing methods of randomizing Sobol' sequences for improving uncertainty of metrics in variance-based global sensitivity estimation," *Reliability Engineering & System Safety*, vol. 210, p. 107499, 2021.